On-site inspection of conservation works using THz TDS

Summary: Sparse deconvolution analysis

1 Sparse deconvolution(SD)

The following description of sparse deconvolution is based on the paper "Terahertz Superresolution Stratigraphic Characterization of Multilayered Structures Using Sparse Deconvolution" by Junliang Dong, Student Member, IEEE, Xiaolong Wu, Alexandre Locquet, and David S. Citrin, Senior Member, IEEE.

If one performs a reflection measurement of a multilayer system, the received signal $\boldsymbol{y}$ in the time-domain will be a convolution of the incident signal $\boldsymbol{h}$ and the impulse-response function(IRF) $\boldsymbol{f}$, with the addition of some noise $\boldsymbol{e}$ (assumed to be gaussian with standard deviation σ). This can be expressed as:

$$\boldsymbol{y} = \hat{H}\boldsymbol{f} + \boldsymbol{e} \tag{1}$$

with $\boldsymbol{y}, \boldsymbol{f}, \boldsymbol{e} \in \Re^n$, n the length of the data points and $\hat{H}$ is the toeplitz matrix where the elements wrap around the borders. $\hat{H}$ is constructed from h. Since $\boldsymbol{f}$ is the IRF of the layered sample it will be zero almost everywhere except at the interfaces between each layer, in other words $\boldsymbol{f}$ is sparse. This leads to equation 2:

$$F(\boldsymbol{f}) = \frac{1}{2}||\boldsymbol{y} - \hat{H}\boldsymbol{f}||_2^2 + \lambda||\boldsymbol{f}||_1 \tag{2}$$

where λ is a regularization parameter, F is the error function to be minimized and $||\cdot||_2, ||\cdot||_1$ is the L2 and L1 norm respectively. By increasing λ the sparsity of $\boldsymbol{f}$ will increase. If λ is increased too much the model might be underfitted which means one will lose sample features. In the same way one can overfit the data, which means noise will dominate the resulting $\boldsymbol{f}$. The regularization parameter is determined through trial and error but one can start from a value which is roughly $\geq 3\sigma||\boldsymbol{h}||_2$ for an initial guess.

The minimum of F can not be determined analytically, but it can be approximated by the iteration given in equation 3.

$$\boldsymbol{f}_{i+1} = S_{\lambda\tau}^{soft}\left(\boldsymbol{f}_i - \tau\hat{H}^T\left(\hat{H}\boldsymbol{f}_i - \boldsymbol{y}\right)\right) \tag{3}$$

where $S_{\lambda\tau}$ is a thresholding function and τ is the stepsize. For thresholding functions based on convex penalty functions this iteration procedure converges to the global minimizer of F. The thresholding function used is shown in equation 4.

$$S_{\lambda\tau}^{soft}(x) = \max\left(|x| - \tau\lambda, 0\right)\operatorname{sgn}(x) \tag{4}$$

Sgn is the usual sign function. The stepsize τ should not be set bigger than $\frac{2}{||\hat{H}^T\hat{H}||_2}$. Also to speed up computations the fact that $\hat{H}$ is a circulant matrix with real entries should be used. This reduces the computational complexity from $\mathcal{O}(n^2)$ to $\mathcal{O}(n \log n)$ since one can then simply perform a FFT of $\boldsymbol{h}$ to find the eigenvalues.

2 Evaluation method

2.1 Setting the reference

Our samples are constructed in a way that the very first layer is relatively thick, so that the pulse originating from the air-first layer surface interface can be isolated. We construct the reference pulse by cutting it out using a 10 % tukey window which is centered around the minimum of the pulse. The minimum of the first pulse is found using a threshold above the noise level. Using the first pulse as reference has the advantage that it is easier to identify the subsequent reflections.

2.2 Deconvolution algorithm

Assuming $\boldsymbol{y}$ and $\hat{H}$ are given, where $\boldsymbol{y}$ is normalized to one and offset corrected. Sparse deconvolution is then perfomed using the following procedure:

1. A λ is chosen based on σ or by guessing
2. The stepsize is set to $||\hat{H}^T\hat{H}||_2^{-1}$
3. For the first iteration $\boldsymbol{f_0}$ is set to the zero vector
4. $\boldsymbol{x} = \boldsymbol{f}_0 - \tau\hat{H}^T\left(\hat{H}\boldsymbol{f}_0 - \boldsymbol{y}\right)$ is calculated
5. $(\boldsymbol{f}_1)_i = S_{\lambda\tau}^{soft}(x_i)$, where x_i are the elements of $\boldsymbol{x}$ and $i = 0, 1, ..., n-1$
6. Steps 4 and 5 are repeated 200 times, updating $\boldsymbol{f}_0$ with the result from step 5.
7. By comparing $||\boldsymbol{f}_i||_1, i = 1, 2, ..., 200$ the most sparse $\boldsymbol{f}_i$ is returned
8. λ can then be varied and the previous steps repeated to adjust the sparsity of the output

3 Resolution limits

To find an upper bound on the spatial resolution of the method, measurements for a varying air gap size were performed and evaluated. The first layer was made of polystyrene in the first set of measurements and in the second set it was a mortar slab. Underneath that a block of more than 5 cm thick polyethylene (PE) was placed. The first layer was fixed on a mount so that the height to the polyethylene block was adjustable making

it possible to vary the air gap between the two interfaces. The width of the gap was controlled using a micrometer screw. For every measurement shown throughout, the Schweissguete system was used. It has a bandwidth of approximately 300 GHz with its intensity maximum at around 50 GHz. The focus was adjusted to the upper layer once and not changed for all measurements shown in this section.

Polystyrene-air-polyethylene

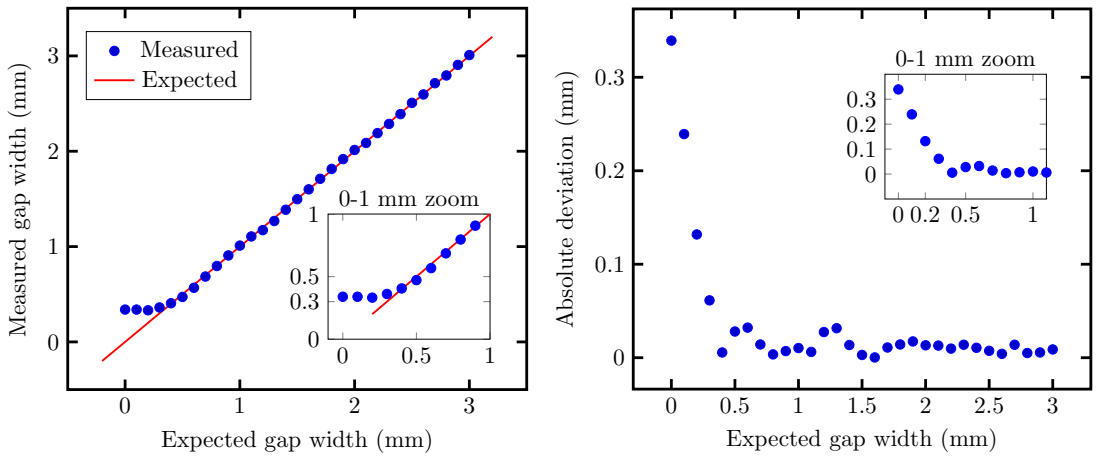

Mortar-air-polyethylene

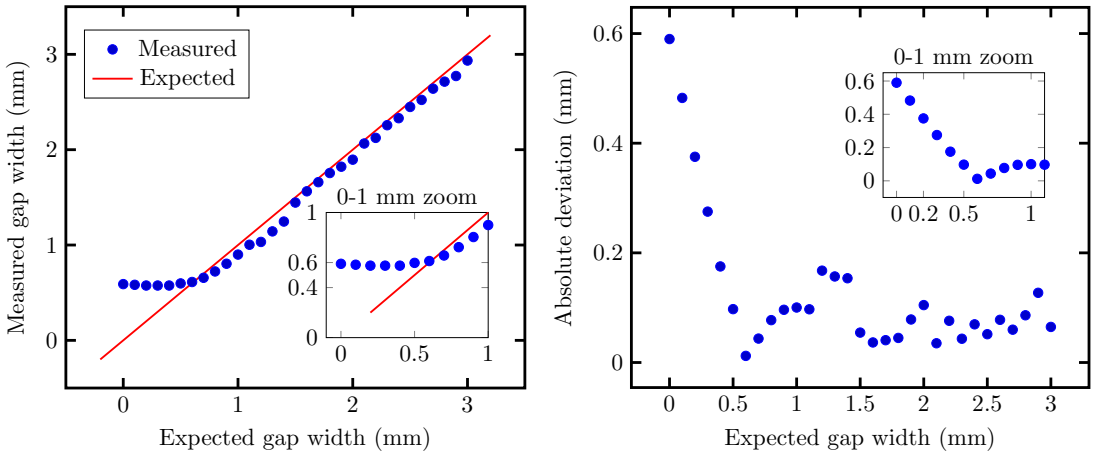

The mortar-air-polyethylene plot shows that the smallest spatial resolution of an air layer between a mortar and polyethylene layer is $\approx 0.6\,\text{mm}$, which corresponds to a delay of $\approx \frac{0.6\,\text{mm}}{0.3\,\text{mm/ps}} = 2.0\,\text{ps}$.
The refractive index of cyclododecane is approximately 1.53. This means that the smallest spatial resolution of a cyclododecane layer is about $\frac{2.0\,\text{ps}}{1.53} \approx 1.31\,\text{ps}$ or $0.39\,\text{mm}$

It can be seen that the resolution for polystyrene is higher than mortar. This is probably because the surface of mortar scatters more of the incident radiation.

4 Mockups

4.1 Sample description

Four mockup samples were prepared by placing approximately 7 mm-thick mortar layers on an aluminum foil. These mortar layers were then covered by a cyclododecan layer of approximately 0.5 mm thickness. Finally, sacrificial render was poured over forming a roughly 7 mm-thick top layer. After the top layer was dry enough to detect the reflection from the aluminum foil at the bottom, the samples were raster scanned 15 times in the following nine months. Figure 1 shows a top view of the wooden frame containing the four mockup samples.

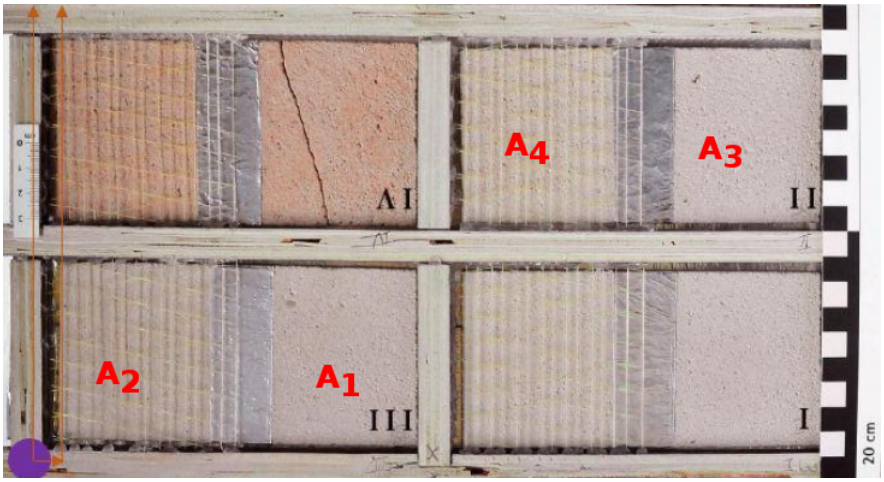

Figure 1: Mockups

4.2 Data sets

In different time intervals over approximately 300 days a full grid scan, also called an image, was taken of the complete frame. Since the measurements were taken over a long time span the coordinate system changed a bit between some images. Though not more than $\pm 5\,\mathrm{mm}$, which could be seen by comparing P2P plots of the complete frame. Because of the fairly long run time only 15 images were evaluated. Four areas were chosen, each containing 20 measurement points. A peak to peak plot helps choosing the areas of interest. Coordinates of the points were not changed for all 15 images. The approximate and exact locations can be seen in Figures 1 and 2 respectively.

4.3 Evaluation

4.3.1 Evaluation remarks

- To get the time difference of the overlapping pulses, the difference between argmin and argmax was determined in the interval where the pulses were expected to be.
- A point was only evaluated if the first of the two overlapping pulses had a phase shift of π relative to the very first pulse and it was required that the second pulse of the double pulse had a phase shift of π relative to the first pulse of the double pulses. This means that not all 20 points were evaluated for some areas.
- For each area the mean was taken of the points used in the evaluation.
- The error bars shown in the following plots were calculated by dividing the standard deviation with the square root of the number of measurements i.e. standard deviation of the mean.
- One has to keep in mind that the time of flight to a point in the plot is twice the actual optical delay, since the radiation has to travel to and back from the sample. All optical delay values shown are already halved to take this effect into account.
- For all areas λ was set to 8. It is kept constant for all traces to ensure comparability.

An example of an evaluation can be seen in Figure 3. The upper plots shows the measured signal $\boldsymbol{y}$, the reference(first pulse only) and the convolution of the reference pulse with the IRF. The bottom plots shows the IRF. Both are plotted against time of flight. Generally two double pulses can be identified in the IRF. If a peak is in the positive direction it means that the phase is the same as the reference. If it is in the negative direction then it is shifted relative to the reference phase. The smaller peaks seen in the IRF are due to noise or other non-sample related phenomena. The number of peaks can be reduced by adjusting λ.

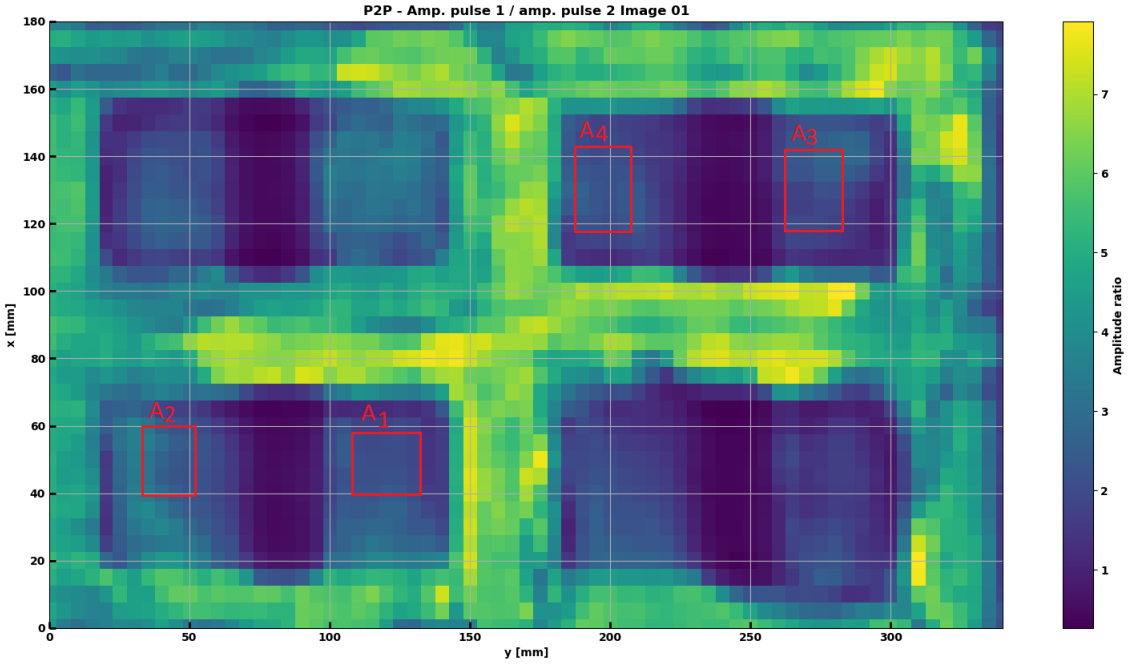

Figure 2: P2P of the first image

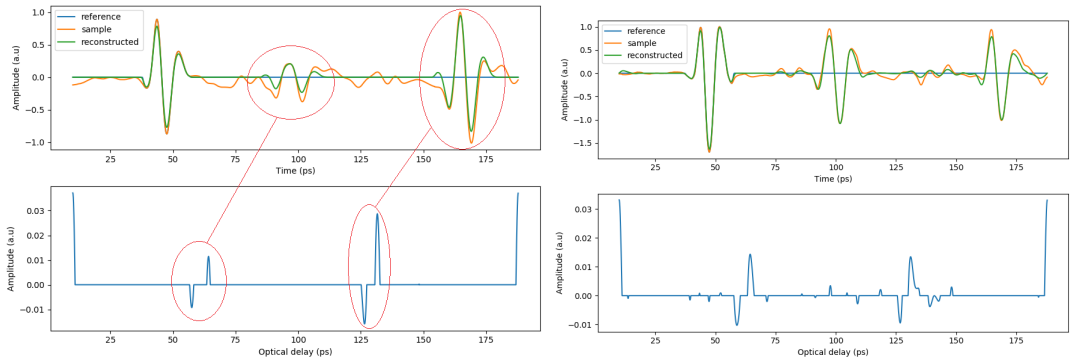

Figure 3: Sparse deconvolution example. The figure to the left is from area 4 after 12 days and the one to the right is from the same area but 264 days later. Left double peak shows the layer in between the two mortar layers consisting of either air or cyclododecane, the right two peaks shows the mortar foil interface. The two left plots shows an example where a lambda of 8 was well suited whereas the two right ones shows one where it did not fit well.

4.4 Results

The IRF generally shows two peaks originating from the mortar-foil interface. One would expect only to see one pulse here since the mortar is placed directly on top of the foil.

Day/Area	1	2	3	4
0	20	19	20	20
3	19	18	20	20
10	20	17	17	20
12	20	17	16	19
20	20	17	15	18
45	20	17	17	20
117	20	18	20	20
153	17	20	20	20
157	17	20	20	20
158	17	20	20	20
160	15	20	20	20
182	16	20	20	20
213	17	20	20	20
255	20	20	20	20
276	20	20	20	20

Table 1: Number of points used for each area and day

The reason for this could be that there is a small air gap, which does not change with time, in between the mortar and the foil. Figure 4 shows plots of the delay between the last two echoes for the evaluated images for each area. One can see that the time delay does not follow a clear trend. The difference in time of flight of the last double pulses did not change significantly, even though the top layer dried and the cyclododecane sublimated. This indicates that the implementation of SD can be used for monitoring changes in the cyclododecane layer. Table 1 shows the number of points that were used in each area and day. More points could be included by lowering λ. But this was not done to have as many parameters constant as possible between the images to ensure comparability. The total delay was calculated taking the mean of the position of the last two peaks, and then comparing the distance to the first pulse. Figure 5 shows the change in the cyclododecane layer for each area in the upper plots and in the lower plots the total time of flight through the mortar. The dashed lines in the upper plots indicate the highest time resolution. One can see that the cyclododecane layer evaporates so that it is replaced with air and therefore a decrease in the time of flight can be seen. Table 2 shows the mean of the first 100 days and for the last 200 for each area. Table 3 shows the difference in the mean value of the days after the 100th day and the first day of the total time of flight. One can see that the change is larger for the total time of flight compared to the gap delay change.

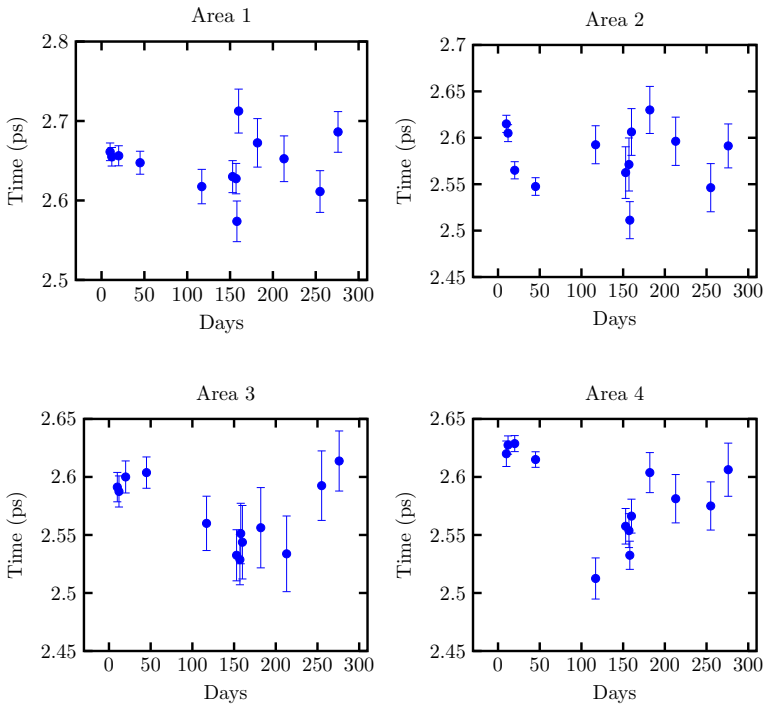

Figure 4: Delay between the two reconstructed pulses originating from the mortar-(air)-foil interface.

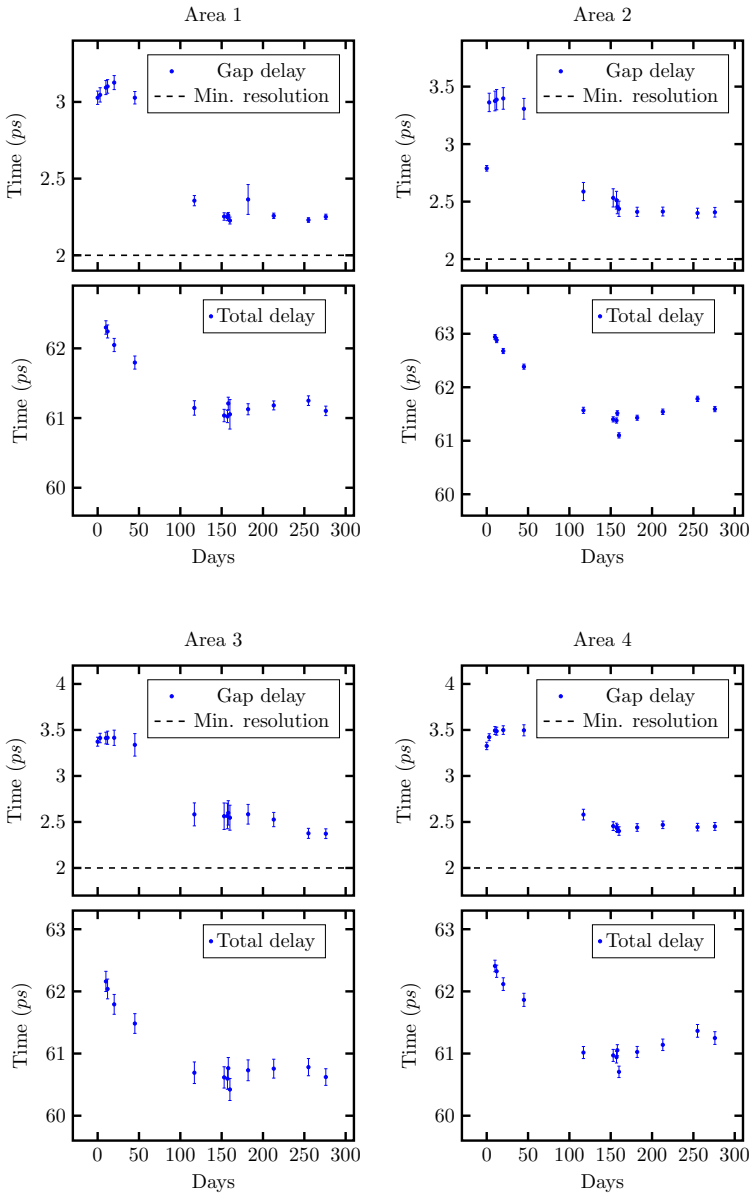

Figure 5: The upper plots, for the four areas, shows the time difference between the first two reflections caused by the mortar-cyclododecane-mortar interface. The dashed line indicates the measured bound on the resolution as discussed in section 3. The lower plots for each area shows the total time of flight through the mortar.

Days/Area	1	2	3	4
< 100	3.1 ps	3.3 ps	3.4 ps	3.5 ps
> 100	2.3 ps	2.5 ps	2.5 ps	2.5 ps
Δ	-0.8 ps	-0.8 ps	-0.9 ps	-1.0 ps

Table 2: Gap delay mean values and the difference between the mean of the first 100 days and the following days

Days/Area	1	2	3	4
0	62.3 ps	62.9 ps	62.2 ps	62.4 ps
> 100	61.1 ps	61.5 ps	60.7 ps	61.1 ps
Δ	-1.2 ps	-1.5 ps	-1.5 ps	-1.4 ps

Table 3: Total time of flight for the first day and mean values of the days after the 100th day. The third row shows the difference between the first day and the mean value.

5 Basilika

In this study we use THz TDS in combination with a sparse deconvolution algorithm for evaluation to verify the sublimation of the connecting cyclododecan layer used in the conservation process of the facade mural paintings on the Roman Imperial Throne Room (Konstantinbasilika), which is part of the UNESCO world cultural heritage site in Trier, Germany. The mural paintings located on the outer facades of the Throne Room have remarkably survived the exposure to the changing weather conditions for centuries. In order to protect them from further degradation, a removable sacrificial render system was applied with a layer of cyclododecan separating it from the original wall with the Roman painting. It is expected that the cyclododecan layer will sublimate with time and an empty spacing between the original wall and the sacrificial render will persist. In order to assess this, three areas of approximately 50x50 mm were selected and raster scanned in reflection geometry using a fiber coupled, portable THz TDS system. The three areas were imaged roughly two weeks after the preservation process was completed and approximately one year later to confirm the sublimation of the cyclododecan layer. The three areas are denoted A, B and C and can be seen in Figure 6. The measurement of area C did not complete though because of high temperature fluctuations causing the laser to lose mode-lock. That data set will therefore be disregarded.

Figure 6: Areas A, B and C from left to right

5.1 Results

The pulses for area A were quite attenuated compared to area B and showed up later in the trace, 50 ps compared to 100 ps for B. This is probably because the wall in this area is thicker compared to B. For area A λ was set to 8 for both years and for area B it was set to 15 also for both years. Otherwise the evaluation was similar to the one used for the mockup data. Table 4 shows the mean values of an area for the delay of the mortar-cyclododecan-mortar layer and the number of points used for each area and year. To get an idea of which points to choose for the evaluation, a peak to peak plot was made for each area and year they are shown in Figure 7.

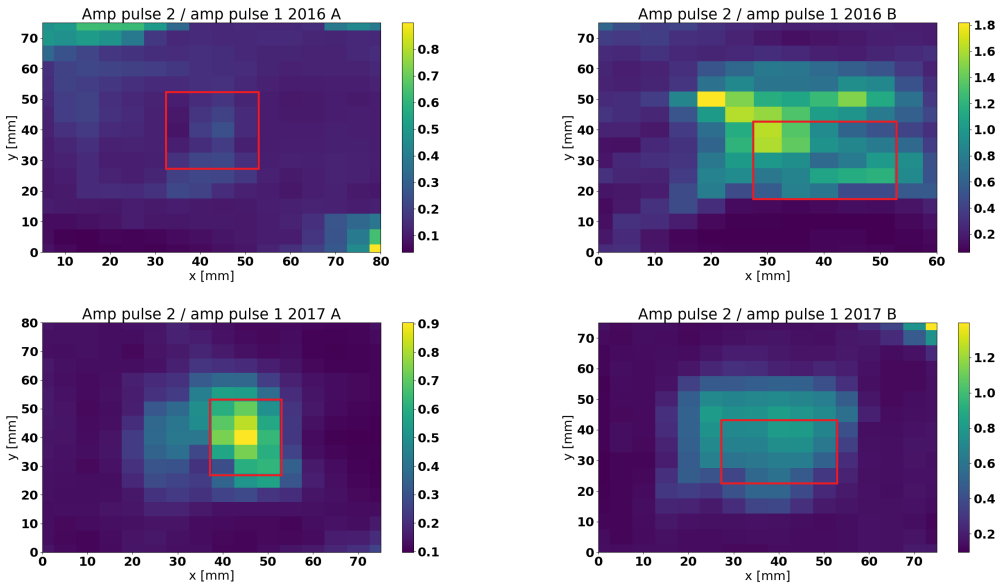

Figure 7: Peak to peak plots of the two areas for 2016 and 2017. The red boxes indicate the points considered for evaluation.

(a) 2016				(b) 2017			
Area	Mean (ps)	St. Dev. (ps)	Count	Area	Mean (ps)	St. Dev. (ps)	Count
A	3.16	0.24	14/20	A	2.68	0.16	12/15
B	3.37	0.41	15/25	B	2.79	0.15	13/20

Table 4: Mean A and B in 2016/2017. Area C was disregarded because of problems during the measurement.

The results presented in Table 4 shows that the time of flight of the pulses in the double pulse has decreased relative to each other, indicating that the cyclododecane layer has changed between the two years. This can be explained by the sublimation of the cyclododecane layer.

Figure 8 shows a trace from area B 2016 and 2017 with additional double pulses right after the initial one and before the right most one. This could indicate that there is a crack in the mortar before the cyclododecane layer. These points can be seen as bright yellow in the peak to peak plot of 2016 B. In the data from 2017 the crack is not as visible but it can still be identified. Something similar does not show in the data of area A.

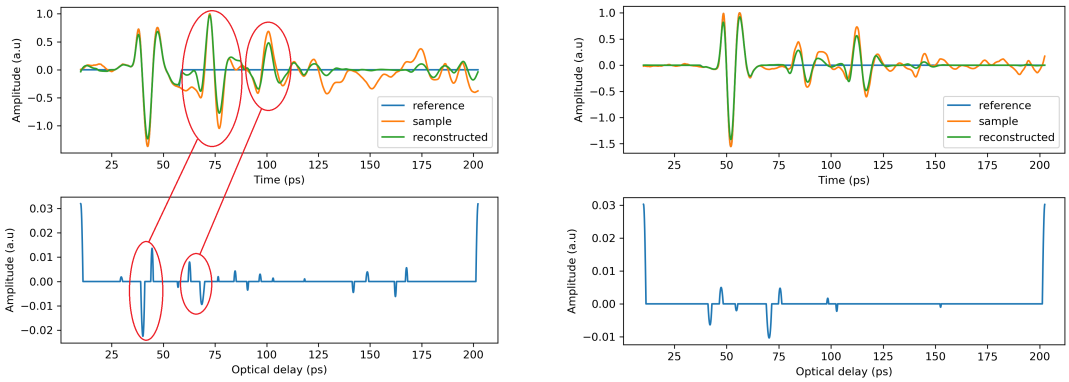

Figure 8: Trace and IRF of a point which possibly shows a crack between the surface and cyclododecane layer. Left plot shows data from 2016, right one from 2017.

The plot to the left shows a discrapancy of the expected phase of reconstructed pulses. The double pulses were expected to have a phase similar to the example shown on the right. The direction of the second double pulse in the left plot indicates that the first reflection comes from an interface of a material with a higher n and followed by a material with a lower n which is unexpected. It could also be that the two pulses are not real double pulses and the reconstructed double peak is just an artifact of the deconvolution (see section 6).

6 Additional comments

A problem with this method is that single reflexes sometimes falsely are identified as double pulses in the resulting IRF. An example of this can be seen in Figure 9 which shows a trace from one of the mortar measurements from Section 3 where the air gap was set to 2.5 mm. The reference used here is not taken from the sample data itself, as was done for all other evaluations, but instead from a previous measurement of a metal foil which was recorded approximately 6 weeks earlier. The largest peak in the IRF shows the reflex from the first surface of the mortar sample. One can see a small negative peak following the large one, which in theory should not be there. The same goes for the double pulse between 100 and 150 ps for which the corresponding peaks in the IRF again are followed by smaller π phase shifted peaks. This phenomena could also be the explanation of the two peaks seen at the mortar foil interface in the mockups data. Figure 10 shows the spread of the peak originating from the surface, i.e the largest peak, to the following peak for the different air gap size measurements ranging from 0 to 3 mm. One can see, similar to Figure 4, that the spread does not depend on the gap size and stays fairly constant over the range, despite the distance from the THz emitter/detector was changing. Table 5 shows the average time of flight and distance of the spread between the double peak showing at the potential mortar-air-foil interfaces for the mockups (Area 1-4). In the last column the average time of flight and distance between the peak from the first reflex and the following peak from the mortar-air-polyethylene data is shown, i.e the average of the points in Figure 10. For the distance calculations a refractive index of 1 was set.

	Area 1	Area 2	Area 3	Area 4	Mortar-air-PE
Distance (mm)	0.79 ± 0.01	0.77 ± 0.01	0.77 ± 0.01	0.77 ± 0.01	0.52 ± 0.003
Time (ps)	2.65 ± 0.007	2.58 ± 0.008	2.57 ± 0.008	2.58 ± 0.005	1.77 ± 0.011

Table 5: Average time of flight and distance, assuming a refractive index of 1, of the spread between the double peak showing at the potential mortar-air-foil interfaces for the mockups (Area 1-4). The last column shows the average of the values of the spread in time and distance between the peak from the first reflex and the following peak from the mortar-air-polyethylene data, where the refractive index is set to 1 for air.

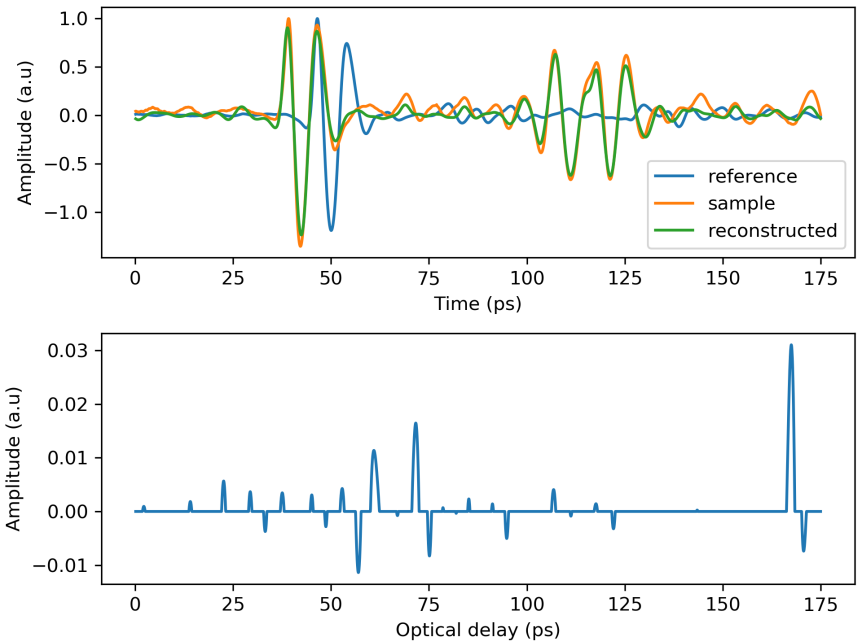

Figure 9: Mortar-air-polyethylene data for an air gap of 2.5 mm. The evaluation is performed using a reference which was measured using an almost fully reflecting metal foil surface. Each peak in the IRF originating from an interface reflection is followed by another phase shifted peak.

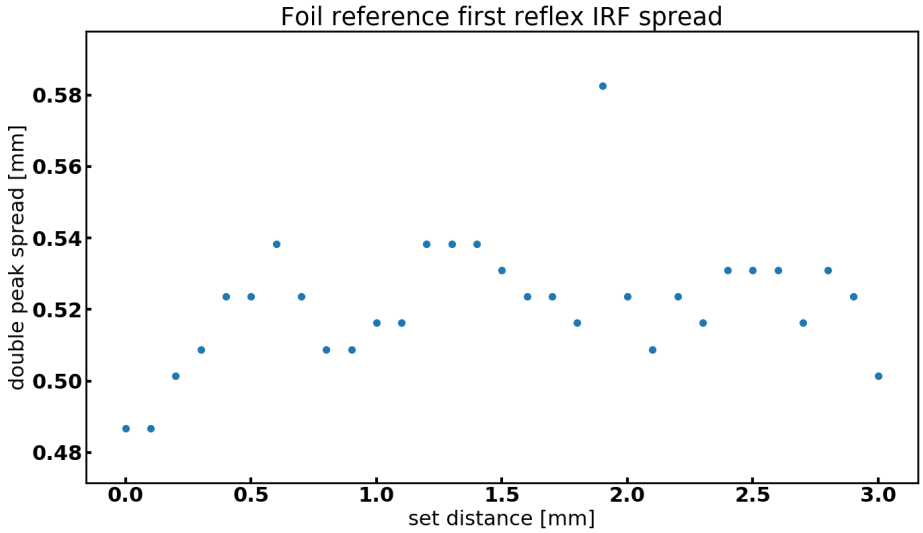

Figure 10: Spread of the peak from the first reflex and the following peak for air gaps ranging from 0 to 3 mm in the mortar-air-polyethylene setup.